



HAL
open science

Effect of surface properties of capillary structures on the thermal behaviour of a LHP flat disk-shaped evaporator

R. Giraudon, S. Lips, D. Fabregue, Laurent Gremillard, E. Maire, V. Sartre

► To cite this version:

R. Giraudon, S. Lips, D. Fabregue, Laurent Gremillard, E. Maire, et al.. Effect of surface properties of capillary structures on the thermal behaviour of a LHP flat disk-shaped evaporator. *International Journal of Thermal Sciences*, 2019, 142, pp.163-175. 10.1016/j.ijthermalsci.2019.04.022 . hal-02120030

HAL Id: hal-02120030

<https://hal.science/hal-02120030>

Submitted on 19 May 2020

HAL is a multi-disciplinary open access archive for the deposit and dissemination of scientific research documents, whether they are published or not. The documents may come from teaching and research institutions in France or abroad, or from public or private research centers.

L'archive ouverte pluridisciplinaire **HAL**, est destinée au dépôt et à la diffusion de documents scientifiques de niveau recherche, publiés ou non, émanant des établissements d'enseignement et de recherche français ou étrangers, des laboratoires publics ou privés.

Effect of surface properties of capillary structures on the thermal behaviour of a LHP flat disk-shaped evaporator

Published in International Journal of Thermal Sciences 142 (2019) pp. 163-175

<https://doi.org/10.1016/j.ijthermalsci.2019.04.022>

R. Giraudon^a, S. Lips^a, D. Fabrègue^b, L. Gremillard^b, E. Maire^b, V. Sartre^a

^a Univ Lyon, CNRS, INSA-Lyon, CETHIL UMR5008, F-69621, Villeurbanne, France

^b Univ Lyon, CNRS, INSA-Lyon, MATEIS UMR5510, F-69621, Villeurbanne, France

Abstract

In this work, capillary structures are manufactured by sintering of copper and zirconia powders using different sintering parameters, in order to obtain porous samples with various hydrodynamic characteristics and surface properties. A specific test bench is designed to reproduce a capillary evaporator of a LHP decoupled from the remaining of the loop and enables the determination of the evaporator heat transfer coefficient and optimum heat flux at the occurrence of the operating limit. The influence of the surface properties on the evaporator thermal behaviour is investigated by polishing the copper wick surface in contact with the evaporator fins, or by coating the zirconia wick with a thin gold layer. It is shown that polishing decreases the thermal performance when the size of the gap between the evaporator fins and the wick becomes lower than the pore size. The coating enables to enhance the evaporator thermal performance, probably by a reduction of the thermal contact resistance or by a favourable surface wettability effect, reducing the strong effect of the wick topography on the optimum heat flux value. Finally, a data mining approach is proposed which highlights the preponderant effect of the surface quality on the evaporator heat transfer coefficient.

Keywords

loop heat pipe; capillary structure; sintering; surface quality; coating; gap; heat transfer coefficient; operating limit; data mining

1 Introduction

The importance of thermal management increases in many industrial sectors, especially in the telecom and computer industries (hardware), where the density of electronic components increases constantly. Consequently, more performant cooling systems, usually based on liquid-vapour phase change phenomena, must be developed to answer these issues. Some of these devices use heat pipe technologies to transfer the heat from a very confined space to a location where space is available for the heat sink. Loop heat pipes (LHPs) are among the most efficient systems. A LHP is a tightly-closed system filled with a two-phase fluid at saturation. It is mainly composed by two transport lines, a condenser and a capillary evaporator.

The key component of the LHP is the capillary evaporator, whose role is to absorb the heat dissipated by the electronic component and to enable the fluid circulation around the loop in a passive way. The evaporator envelope, usually metallic, contains a reservoir of liquid, a porous wick, located close to the inner wall and a series of small channels for the vapour evacuation. As explained by Ku [1] and Maydanik [2], the wick ensures a double role of hydraulic and thermal barrier. The channels may be arranged in the wall or in the wick, with a regular spacing, so that an alternation of contact and non-contact area is observed. When heat is supplied to the evaporator, menisci are formed in the wick, saturated with liquid, generating the required capillary pumping pressure.

The evaporator has to be designed so that heat is transferred from the heat source to the evaporating menisci with the minimum thermal resistance, so that the evaporating surface area has a maximum value, and so that the vapour can be easily removed from the evaporation zone. Hence, various designs have been proposed in the literature [3]. Most numerical and experimental studies focusing on LHP evaporators aim at understanding the physical mechanisms affecting their behaviour, as well as the effects of numerous parameters on the evaporator thermal performance. The wick characteristics and especially the permeability and the pore radius distribution plays an important role in the operation and the performance of the LHP (Yeh et al. [4]). In a previous study, Giraudon et al. [5] presented an approach to design and manufacture specific capillary structures for loop heat pipes. They highlighted the links between the manufacturing parameters and the wick properties and the importance to control the whole process in order to fulfil the specifications. They also studied the influence of the wick properties on the thermal behaviour of a LHP capillary evaporator and especially on the maximum heat transfer coefficient between the evaporator wall and the working fluid and the maximum heat flux that can be transferred before the occurrence of the wick dry-out [6]. They concluded that the capillary limit and the boiling limit can both lead to the wick dry-out depending on the wick properties. However, no direct trends could be found concerning the effect of the wick properties on the value of the heat transfer coefficient between the evaporator wall and the working fluid.

The thermal performance of a LHP evaporator is indeed strongly affected by the morphology and topography of the porous surface in contact with the evaporator. In terms of morphology, two major parameters were studied in the literature: the type and location of the grooves collecting the vapour phase, which can be engraved in the evaporator wall or in the porous wick itself, and the quality of the contact between the fins and the flat surface. The type and location of the grooves is widely discussed in the literature, for instance by Maydanik *et al.* [7] for complete LHPs or by Choi *et al.* [8] at the scale of an isolated evaporator. The latter proposed to interpenetrate the wick with the evaporator wall in order to increase their contact surface area. With the proposed design, they found a large enhancement of the evaporator thermal conductance and lower operating temperatures.

The study of the effect of the quality of the contact between the fins and the flat surface is more recent and is still the subject of strong scientific discussion. In classical numerical and theoretical studies, the best configuration is assumed to be a perfect contact between the surfaces, so that the thermal contact resistance is minimum. However, in more and more experimental studies, it is found that an imperfect contact, it means when surfaces are not flat or when the surfaces are even not directly in contact can exhibit better thermal performance than a more classical configuration. For instance, Khammar *et al.* [9] found that the presence of a gap between the flat evaporator and the fins enables to increase the maximum heat load. They showed that 600 μm is the optimum gap enabling the vapour to leave the grooves without increasing the thermal resistance. However, in their study, they did not link the transition gap to the pore radius. Schertzer et al. [10] studied the influence of a gap between the finned evaporator and the porous wick on the heat and mass transfer. They showed that increasing the gap size d_{gap} up to 500 μm had a positive influence on the heat transfer coefficient. The presence of a gap changes the evaporation dynamics. Below 200 μm , a vapour pocket builds up beneath

the porous medium before leaving the evaporator through the grooves. The maximum heat load that the evaporator can evacuate does not exceed 100 kW/m² in this configuration. Above 200 μm, the vapour easily leaves the region between the evaporator wall and the porous medium. Thus, the maximum heat load can reach up to 220 kW/m². In this study, the transition gap has the same size as the pore size. It could indicate that the gap must always be larger than the pore size of the porous structure. A possible physical explanation of the existence of a transition gap was proposed by Platel *et al.* [11]. At start-up, if the grooves are full of liquid, the vapour formed under the fin is evacuated by the channel having the largest diameter, for which it is easier to overcome the capillary pressure difference. If the pore diameter is larger than the gap, dry-out of the wick occurs. Figus *et al.* [12] numerically studied the influence of a thin gap between the fin and the wick. Like the previous authors, they showed that this gap can enable the vapour to leave more easily the grooves, reducing significantly the evaporator temperature. More recently, Nishikawara and Nagano [9] developed a mathematical model to investigate the heat transfer characteristics of a capillary evaporator with a micro-gap between the case and the wick. The model was validated by comparison with experimental results obtained for a polytetrafluoroethylene/ethanol loop heat pipe. Both approaches indicate the existence of an optimal gap between 0 and 50 μm, for which the heat-transfer coefficient is maximum. The reason considered by authors is the following: at high heat flux, the gap prevents a vapour pocket from forming in the wick, and at low heat flux, the evaporation interface is larger.

If the fact that a gap can improve the LHP evaporator performance begins to be understood, further studies are still required to fully understand the role of such a gap depending on the operating parameters. The phenomena occurring at the microscale at the contact between the fins and the evaporators walls are indeed often conjectural and specific experimental studies are required. Some authors are trying to visualize the liquid-vapour interface directly in the LHP. For instance, Kumar *et al.* [13] and Odagiri *et al.* [14] performed recently IR visualisation at the microscale and observed directly several behaviour of the evaporator, in terms of the presence, or absence, of liquid bridges at the contact between the fins and the evaporator. They proposed different heat transfer phenomena, occurring when the heat flux increases: evaporation of the menisci located at the boundary line between the heating wall, the wick and the channel; nucleate boiling at the contact surface between the wall and the wick and evaporation of the microlayers; evaporation at the menisci located inside the wick. The heat transfer coefficient is the highest when a liquid bridge exists between the fins and the evaporator and decreases when a vapour layer is formed at the interface, which can be in contradiction with the role of a gap described by other authors.

As a conclusion, all these studies showed that the surface contact quality between the evaporator fins and the porous structure has an influence on the heat transfer. It must exist a trade-off between the presence of a gap, its size, and a globally good thermal contact between the fins and the evaporator. However, at the author's best knowledge, the effects of the porous surface properties at the vicinity of the evaporator fins, i.e. surface quality, surface hardness, surface wettability or thermal conductivity, were not investigated yet. This surprising lack of knowledge of the effect of the surface topology (in contrast with its morphology) prevents to optimize the manufacturing techniques involving multilayer wicks. For instance, Choi *et al.* [15] developed manufacturing techniques to increase the capillary pressure of wick without reducing its permeability, but no information on the effect on the heat transfer coefficient is predictable yet.

In the present paper, an experimental study focusing on a flat disk-shaped LHP evaporator is proposed. Various copper and zirconia porous structures have been manufactured by a sintering method and characterized, and then tested in a specific test bench reproducing a LHP evaporator without the coupling with the remaining part of the LHP. Two parameters are specifically studied: the topography of the porous surface in contact with the evaporator fins and the addition of a very thin gold layer on the wick surface, modifying the surface wettability, its hardness and the thermal conductivity of the porous structure at the contact with the fins. The influence of the modification of the surface properties on the maximum heat load and on the heat transfer coefficient is analysed.

In a first section, the manufacturing and the characterisation procedures of the porous structures are detailed. Then, the results of the thermal analysis are presented and analysed. Finally, an analysis using data mining is proposed to go further in the comprehension of the thermal behaviour of a capillary evaporator.

2 Manufacturing and characterisation of the porous samples

2.1 Manufacturing procedure

In the present study, porous structures were manufactured by sintering of copper and zirconia powders using different sintering parameters, and characterised in terms of thickness, porosity, permeability and effective pore radius. The manufacturing procedure is detailed in Giraudon *et al.* [5]. The powder is pressed in a cylindrical matrix by two pistons leading to a 40 mm diameter flat disk. Then, the disk is sintered in a furnace. Copper disks are sintered during 30 min at 900 °C and zirconia disks during 120 min at 1230 °C. In the present study, twelve samples are considered. Ten samples made of copper are named Cu-x-y. x , ranging from 1 to 8, is a number corresponding to a given set of manufacturing parameters [6]. y is a letter (a, b, or c) corresponding to various samples made with the same set of manufacturing parameters. Two samples made of zirconia are called Zi-1 and Zi-2. All samples were characterised in terms of diameter, mass, thickness, porosity, effective pore radius and permeability following the procedures presented in Giraudon *et al.* [5]. Moreover, a topographical characterisation was also performed on each sample by means of confocal microscopy.

2.2 Topographical characterisation

To characterise the surface topography, the wick surfaces were scanned on both faces with a confocal microscope (*Stil*®, France). The profile (vertical axis z) measured along the diameter (horizontal axis x) enables to estimate the roughness. The optical sensor has a vertical measuring range along the z axis of 350 μm and accuracy lower than 1 μm in the x and z directions. It appears that the manufacturing procedure leads to different topographies on the two faces of each sample. One side is convex whereas the other side is concave. The main reason explaining this difference is the slightly asymmetric shrinkage observed during sintering (due to slight green density differences between top and bottom of the disks after pressing). Figure 1 presents an example of topography analysis of a convex side (a-c) and a concave side (d-f). Tests with pressure paper highlighted the effect of the surface geometry on the contact between the samples and the wall of the LHP evaporator (pictures c and f). The flatness of each side was measured and corresponds to the maximum altitude difference between the centre and the edge of the sample. It can be positive (convex side) or negative (concave side).

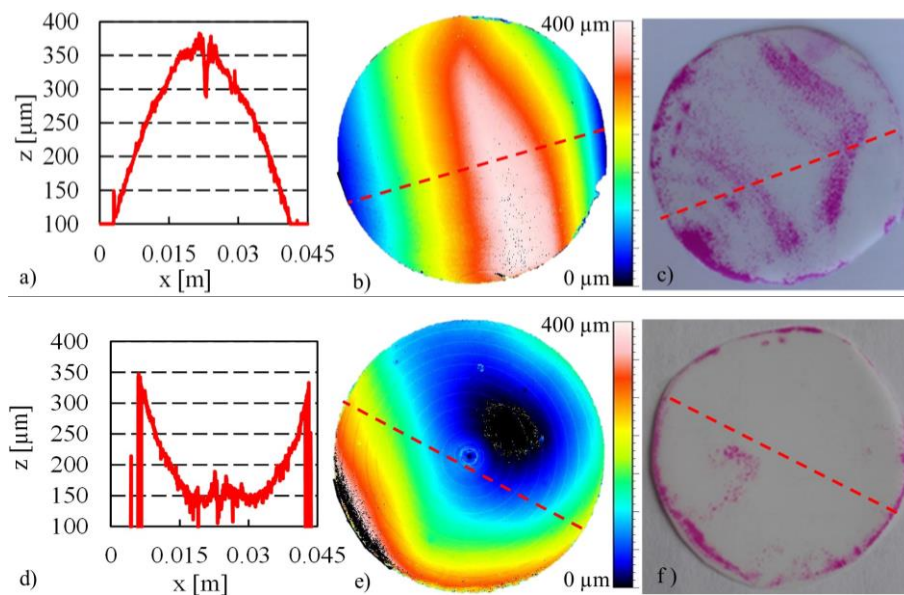


Figure 1 : Examples of topography analysis by confocal microscopy (profile (a, d) and complete surface (b, e) and with pressure paper (c, f) of the convex side of sample Cu-7-c (a, b, c) and the concave side of sample Cu-2-c (d, e, f)

2.3 Description of the surface treatments

The topography of various samples was modified by surface treatments to investigate the influence of this parameter on the evaporator thermal behaviour. For instance, the sample Cu-7-c was submitted to various surface polishing procedures in order to modify its topography, and then characterized (surface topography, thermal and hydrodynamic properties) after each of these preparation steps. Figure 2 (a) shows the profile of each side obtained before the surface polishing. A large difference between the sides A and B is observed: they have a similar roughness but the side A is convex whereas the side B is concave. Machining by means of a turning machine enabled to obtain a flat sample but increased the roughness (Figure 2 b). Sanding with a 300 then 600 grit paper reduces the roughness but created a dome (Figure 2 c). Finally, polishing with a *Lamplan* flat polisher (LAM PLAN M.M. 8400™) reduced the roughness and provided an excellent flatness but the top and bottom surfaces were not parallel anymore (Figure 2 d). Surface treatments were also performed on other samples in order to check the robustness of the results but they are not detailed here.

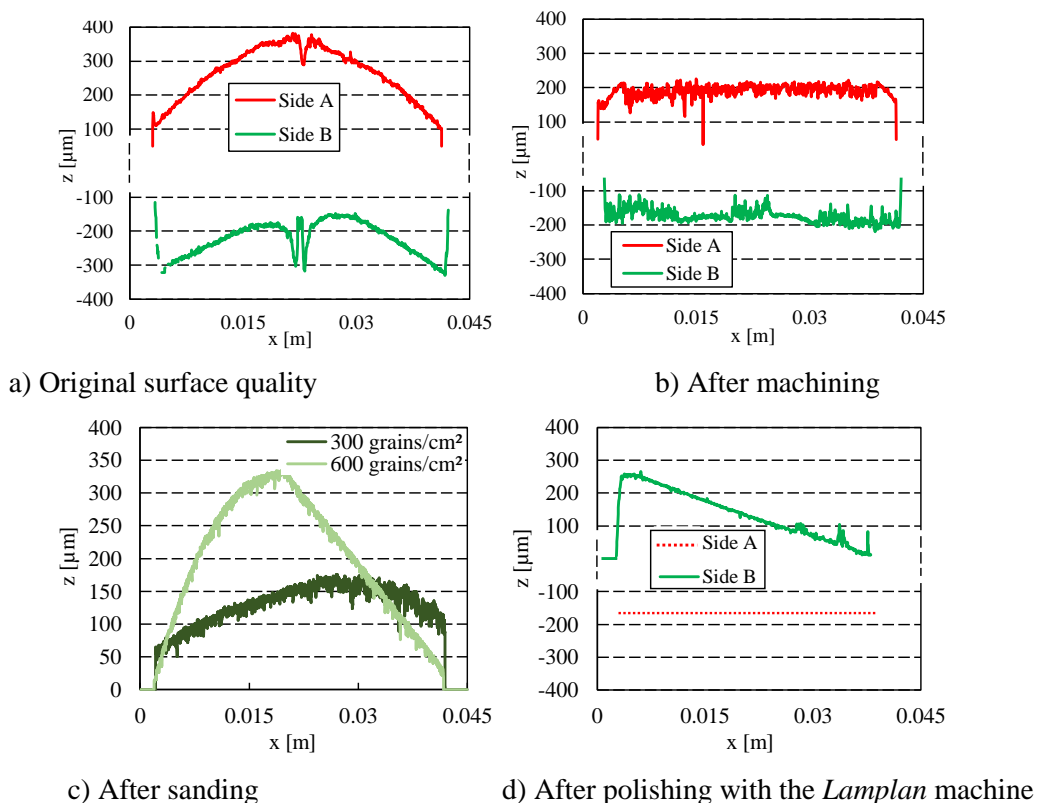


Figure 2: Surface profiles along a diameter of sample Cu-7-c before and after various treatments

2.4 Deposition method of the gold coating on samples Zi-1 and Zi-2

In order to separate the effect of the surface topography and the one of the other surface properties (wettability, hardness, and thermal conductivity), the two zirconia samples were coated with a thin gold layer. The sample topography as well as the hydrodynamic characteristics remained unchanged before and after the coating due to the low thickness of the gold layer (thinner than $0.1 \mu\text{m}$). The effect of the coating was studied on the concave side of sample Zi-1 and on the convex side of sample Zi-2, since the influence of the coating may depend on the sample topography. The gold layer was applied by sputtering. The sample was located inside a metal coater. The pressure was decreased down to $4 \cdot 10^{-2}$ mbar. Then, Argon was added. A strong electric power was applied between a gold target (cathode) and the sample (anode). Under the effect of the electric power, the Argon ions hit the gold target and eject gold atoms that are deposited in the whole chamber, and in particular on the sample. For each coater, the thickness of the gold coating depends on the distance between the target and the top layer, on the electrical current and on the coating time. The tests have been conducted with a coater *BAL-TEC SCD*® and the following coating parameters: 60 mA during 200 s and at a distance of 50 mm. It leads to a theoretical gold coating thickness of 75 nm.

2.5 Hydrodynamic characterisation

The hydrodynamic characterization of each sample was performed following the procedure described in [5]. The porosity was determined by measuring the volume and the mass of each sample. The permeability and effective pore radius were determined by means of a specific test bench developed by the authors. The permeability is determined by measuring the relation between the liquid mass flux in the wick and the pressure difference across the wick whereas the effective pore radius measurement relies on the maximum height of a liquid column the wick can stand without depriming.

2.6 Thermal characterization

The test bench designed in order to characterise the thermal behaviour of the manufactured samples is the same that the one presented in [6]. Its main characteristics and the experimental procedure are summarized in the present section for the sake of clarity. The test bench aims at reproducing the configuration and the operation of an evaporator in a flat LHP, by decoupling it from the transport lines and the condenser. It consists of a double-wall glass enclosure secured at the base by a clamping ring (Figure 3). A grooved evaporator and the porous wick are embedded into the cylindrical part of the base. An L-shaped tube (vapour tube) goes through the base wall to enable the vapour to flow from the grooves to the enclosure containing the fluid at liquid-vapour equilibrium.

The saturation temperature of the fluid is controlled by a cryogenic fluid flowing in the annular space of the enclosure. The liquid level H_l can be modified by opening the filling valve in order to adjust the hydrostatic pressure ΔP_{hs} applied on the wick. Two thermocouples, housed inside a stainless steel sealed shell to ensure the sealing of the system, measure the saturation temperature: one in the liquid phase (T_l) and the other in the vapour phase (T_v). The saturation temperature is calculated as the average between the two values when the absence of non-condensable gazes is confirmed (i.e. when the temperature difference between the two thermocouples is lower than their uncertainty). In the present study, the saturation temperature is set to 50 °C with water and 40 °C with pentane, and the level of liquid is kept constant and equal to 3.9 cm. Note that it had been shown in [6] that this parameter affects only slightly the thermal behaviour of the samples as the hydrostatic pressure difference induced by the level of liquid is small compared to the capillary pressure that the porous sample can provide.

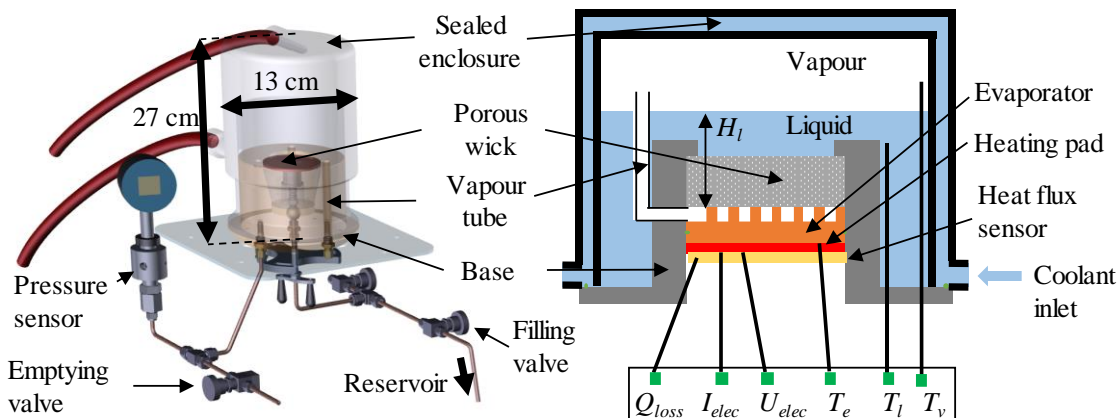


Figure 3 : Schematic of the experimental apparatus

The evaporator is made of a flat disk-shaped copper block, with a diameter of 40 mm and a thickness of 8 mm. Nine 2 mm wide and 1.5 mm deep grooves were engraved in the copper block. They are separated by 1.5 mm thick fins. The wick is located above the grooved copper block. A thermocouple having a diameter of 80 μm is located inside a 0.8 mm thin groove engraved in the bottom surface of the evaporator. A heat flux ranging from 0 to 150 W (12 W/cm^2) is supplied by a heating pad located between the evaporator wall and a heat flux sensor. This sensor enables to measure the part of the heat flux lost through the back of the heat source. The heat load effectively supplied to the evaporator is determined by subtracting the lost heat power Q_{loss} to the fixed electric power:

$$Q_{in} = U_{elec}I_{elec} - Q_{loss} \quad (1)$$

where U_{elec} is the voltage and I_{elec} the current intensity of the heating element.

The heat transfer coefficient h_e between the evaporator wall and the evaporating fluid is defined as follows:

$$h_e = \frac{Q_{in}}{S_w(T_e - T_{sat})} = \frac{Q_{in}}{S_w\Delta T_{sh}} \quad (2)$$

where T_e is the evaporator wall temperature, T_{sat} is the saturation temperature of the fluid and S_w is the cross-sectional surface area of the wick, equal to 12.6 cm² with the present samples. The temperature difference between the evaporator wall and the fluid at saturation is called the wall superheat ΔT_{sh} .

The absolute uncertainties are of about 3 W on the heat fluxes, 5 % on the porous wick area and 1 K on the wall superheat. The relative uncertainty associated to the heat transfer coefficient can reach 30 % at low heat loads, due the small temperature difference between the evaporator wall and the vapour phase and due to the small subcooling of the liquid, making difficult the estimation of the saturation temperature. At high heat loads, it decreases down to 10 %.

During the tests, the heat load is increased step by step, a steady state being reached before applying the next step. The test is stopped when the evaporator temperature reaches 120 °C in order to protect the test bench materials against overheating. Figure 4 shows an example of thermal behaviour exhibited by a manufactured sample, in which the heat transfer coefficient h_e and the superheat ΔT_{sh} between the evaporator wall and the vapour phase are plotted as a function of the heat load. At low heat loads, the heat transfer coefficient remains constant up to a value called Q_{opt} from which it drastically decreases, leading to a large increase of the evaporator temperature T_e . The heat transfer coefficient recorded at Q_{opt} is called the optimum heat transfer coefficient $h_{e,opt}$ and the temperature difference is called the maximum superheat $\Delta T_{sh,max}$. When the heat load is greater than Q_{opt} , small bubbles can sometimes be observed at the top surface of the porous structure. Clearly, an operating limit is reached at Q_{opt} , leading to a degradation of the heat transfer.

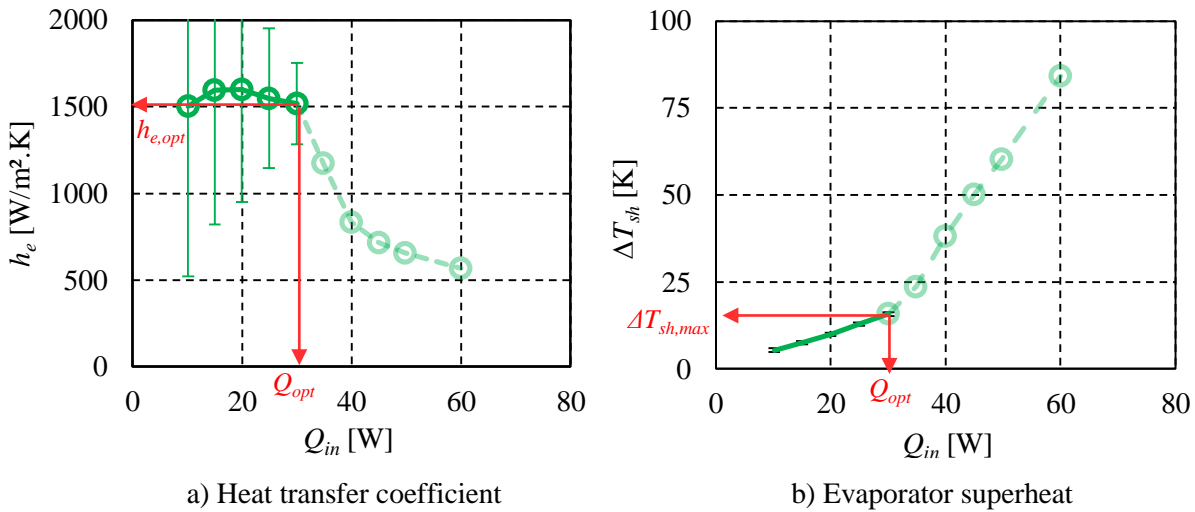


Figure 4: Example of variation of the heat transfer coefficient (a) and of the evaporator superheat (b) as a function of the heat load

Various phenomena can lead to the dry-out of the evaporator and to the sudden drop of the heat transfer. The occurrence of the capillary limit and the boiling limit was discussed in [6]. The capillary limit is reached when the pressure drops through the wick ΔP_w and the vapour tube ΔP_{vt} overcome the sum of the maximum capillary pressure and the hydrostatic pressure ΔP_{hs} of the liquid column of height H_l above the wick surface. The theoretical capillary limit $Q_{opt,th}$ is determined by equalising the pressure drops and the capillary force added to the hydrostatic pressure, leading to:

$$\Delta P_{cap,max} + \Delta P_{hs} = \Delta P_w|_{Q_{opt,th}} + \Delta P_{vt}|_{Q_{opt,th}} \quad (3)$$

The evaluation of the various pressure drop and the knowledge of the wick properties enable an estimations of the capillary limit by means of the method presented in [6].

The boiling limit, reached when the superheat between the evaporator wall and the saturation temperature of the fluid inside the porous sample is high enough so that nucleation can start, is here calculated using Chi's equation [16]:

$$\Delta T_{sh,max} = T_l - T_{sat} = \frac{2\sigma T_{sat}}{\rho_v h_{lv}} \left(\frac{1}{r_n} - \frac{1}{r_p} \right) \quad (4)$$

This equation depends on the nucleation radius r_n which must be known. Griffith and Wallis [17] carried out many nucleation experiments with water. They reported nucleation radius varying between 2.5 μm and 25 μm . However, Chi [16] explained that in absence of NCGs, in conventional heat pipes, the nucleation radius could be smaller and reach 0.25 μm . The determination of the boiling limit requires the knowledge of r_n and r_p , which are very difficult to measure accurately. In the present study, r_p is considered to be equal to $r_{p,eff}$, determined by the dedicated test bench. The value of r_n was estimated in [6] by comparing the experimental working limit to the theoretical capillary limit. When the theoretical capillary limit was far from being reached, it was assumed that the boiling limit was reached and the corresponding nucleation radius was calculated. By this way, r_n was estimated to be equal to 0.7 μm for pentane. As a consequence, the boiling limit presented in the present paper is only a rough estimation based on this assumption.

3 Results and discussions

In this section, the thermal behaviour of the various samples are discussed and the effect of the porous surface properties on the heat transfer coefficient are analysed by two different ways. In a first part, a parametric analysis is performed by comparing the thermal behaviours of samples having similar characteristics but different surface properties, because of either a surface treatment or a surface coating. In a second part, the experimental database is extended and a datamining analyses is proposed in order to hierarchize globally the various parameters affecting the heat transfer coefficient.

3.1 Parametric analysis of various effects of the porous surface properties on heat transfer

3.1.1 Topographic and hydrodynamic characterization of the samples

In order to study the surface properties on the thermal behaviour of a LHP evaporator, the various samples were submitted to the surface treatment described in section 2.3. This treatment can also affect the hydrodynamic characteristics of the samples and Table 1 summarizes the properties of the various samples before and after the surface treatments. Some data are missing because of the breakage of some samples before their complete characterization could be performed. The link between the set of manufacturing parameters and the porosity, permeability, effective pore radius and thickness was already presented in [5] and is not discussed in the present paper. However, it can be seen that the surface treatment can affect these parameters, except the porosity :

- In a logical way, the thickness decreases after each polishing. After the last one, for example, the sample Cu-7-c is 35 % thinner than the original sample.
- The permeability of the samples can be affected by the surface treatment if some superficial pores are clogged during the process. It can be avoided during the sanding and the machining but the polishing with the Lamplan machine seems to always lead to an obstruction of the external face of the wick by the wasted copper powder. The very small effective pore radius of the polished samples compared to other samples tends to support this conclusion. The polished samples were immersed in an acidic solution in order to dissolve the grains that may obstruct the smallest pores. However, this chemical treatment had not a significant influence on the permeability. Thus, the polishing by the *Lamplan* machine was considered as non-consistent for the improvement of the evaporator performance sample, and was not taken into account in the following study.
- Except for the polished samples, the effective pore radius is almost not affected by the surface treatment which tends to show that even if some material of the porous structure is removed during the process, no deformation of the superficial pores occurs.

As a conclusion, the surface treatments enabled to change drastically the surface properties in terms of roughness and flatness without drastically modifying the permeability and effective pore radius of the samples. It thus enables a direct comparison of the thermal behaviour of the samples before and after each surface treatment.

Table 1: Summary of the sample properties before and after the surface treatments

Material	Sample	ε [%]	Surface treatment	K [10^{-14} m ²]	$r_{p,eff}$ [μ m]	e_w [mm]	Side flatness type	Flatness [μ m]	Roughness [μ m]
Copper	Cu-1-b	39.3	WT	11.6	11.3	3.2	Convex	100	15
	Cu-2-b	26.7	WT	2.57	23	2.95	Convex	250	30
	Cu-2-c	27.1	WT	1.37	11.5	2.8	Convex	300	15
			S300	1.82	18.5	2.7	Concave	-200	15
	Cu-3-a	40.6	WT	10.1	18.2	5.2	Concave	-200	10
			S300	1.82	18.5	2.7	Convex	300	10
	Cu-4-a	22.6	WT	0.6	5	4.7	Convex	160	10
			P	0.12	5	4.45	Flat	50	5
	Cu-5-a	37	WT	10.5	10.2	2	Concave	-60	5
			S300	0.26	5	1.9	Convex	270	5
			A	3.25	30.7	1.9	Flat	0	10
	Cu-6-c	28.6	WT	0.52	9.2	2.1	-	-	10
	Cu-7-b	37	WT	18.8	52.1	5.6	-	-	-
	Cu-7-c	41.8	WT	16.9	11.5	6	Convex	350	5
			M	19.5	11.5	5.8	Concave	-150	5
							Flat	0	40
18				11.5	4.45	Flat	0	30	
						Convex	60	20	
S600			26.8	11.5	4.2	Convex	320	15	
P	0.43	7.1	4	Convex	320	15			
Cu-8-a	22.4	WT	0.56	11.3	5.45	Concave	-80	5	
						Convex	200	5	
Zirconium	Zi-1	33.7	Coated	1.33	18.4	5.6	Concave	-	-
	Zi-2	30	Coated	0.57	6.6	5.5	Convex	-	-

WT: Without surface treatment; S300/S600: Sanded with a grain density of 300/600 gr/cm²

P: Polished with the Lamplan polisher; M: Machined with the turning machine; A: Immersed in an acidic solution

3.1.2 Effect of the pressure on heat transfer

The evaporator and the heating pad are pressed against each other with a spring in order to reduce as much as possible the thermal contact resistance between these two components and thus, to reduce the heat losses by the back face of the heating pad. As the flatness of the samples are affected by the surface treatment, the pressure repartition between the evaporator and the wick can also be affected. To check if this parameter has an effect on the heat transfer, the influence of the pressure applied by the spring is investigated on the Cu-sin-4-a sample operating with pentane. Figure 5 shows the evolutions of the heat transfer coefficient and the wall superheat with the heat flux at pressures of around 5 kPa and around 30 kPa. The variation of the applied pressure does not significantly change neither the optimum heat flux nor the heat transfer coefficient. In the following, the pressure is set to about 30 kPa in order to reduce the thermal resistance between the heating pad and the evaporator and thus, reduce the heat losses by the back face of the heating pad. The variation of thermal behaviour between the various samples are thus only due to the topographic properties of the sample surface, and not to the potential variation of pressure between two samples.

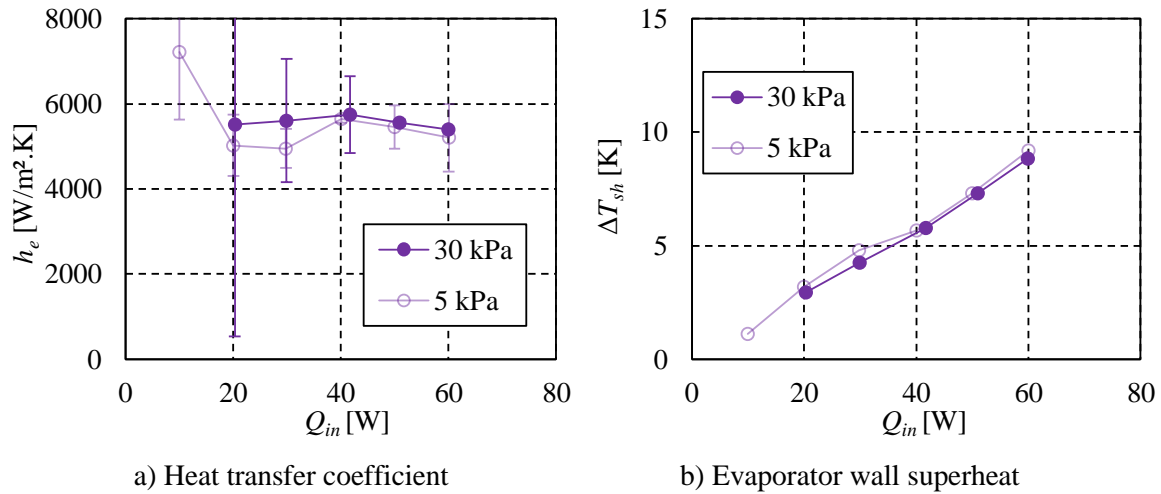


Figure 5: Influence of the pressure applied on the back face of the evaporator (Cu-sin-4-a sample, pentane, $T_{sat} = 40$ °C)

3.1.3 Effect of the wick surface topography on the evaporator thermal behaviour

The effect of the hydrodynamic characteristics of the samples on their thermal behaviour was already presented and discussed in [6] and it appeared that a sample with a low permeability will reach the capillary limit first whereas samples with a high porosity reach the boiling limit first. Consequently, knowing the permeability, the thickness and the effective pore radius, enables the estimation of the operating limits. Pentane and water were compared and it appeared that the heat transfer coefficient is significantly higher with pentane than with water, probably because of the higher wettability of pentane, allowing the fluid to wet more easily the wick in contact with the evaporator wall.

However, no direct link could be drawn between the hydrodynamic parameters and the heat transfer coefficient between the evaporator wall and the working fluid. It was supposed that the observed variations of h_e could be due to surface effects.

To check this hypothesis, the thermal behaviour of the evaporator in which sample Cu-7-c is integrated is investigated in the present study before and after the various surface treatments. Pentane is used as the working fluid as it exhibits better thermal performance than water. Figure 6 shows the evolutions of the heat transfer coefficient as a function of the heat load after each surface treatment of the sample. The experimental heat transfer coefficient, superheat and optimum heat flux are drastically affected by a variation of the surface quality, meaning that this parameter has a significant influence on the evaporator thermal behaviour.

Table 2 summarizes the geometrical and hydrodynamic characteristics as well as the experimental optimum heat flux and the theoretical one corresponding to the capillary limit, the experimental maximum superheat and the one corresponding to the boiling limit, and the optimum heat transfer coefficient of sample Cu-7-c, after the various surface treatments. It can be observed that the flattest surfaces (machined sample and sample sanded with 300 grains/cm²) have the lowest heat transfer coefficient and optimum heat load whereas the concave side of the sample without treatment has the best performance. The samples with a domed surface (convex side of the sample without treatment and sample sanded with 600 grains/cm²) have intermediate performance. The hydrodynamic characteristics after each treatment remaining identical, they cannot cause the observed variations.

Except for the concave side of the sample without surface treatment, which may have reached the capillary limit, the boiling limit probably limits the operation of the polished sample. Indeed, the theoretical capillary limit varies from 102 W for this sample side to 229 W for the sample sanded with 600 grains/cm². These values are much higher than the experimental data: $Q_{opt,exp}$ is lower than 80 W, except for the concave side without surface treatment for which it is of 100 W. On the contrary, whatever the surface treatment, the theoretical superheat to initiate boiling is of 9.8 K in these conditions, while $\Delta T_{sh,max,exp}$ almost reaches or exceeds this value in each test. It means that the boiling limit was more likely reached.

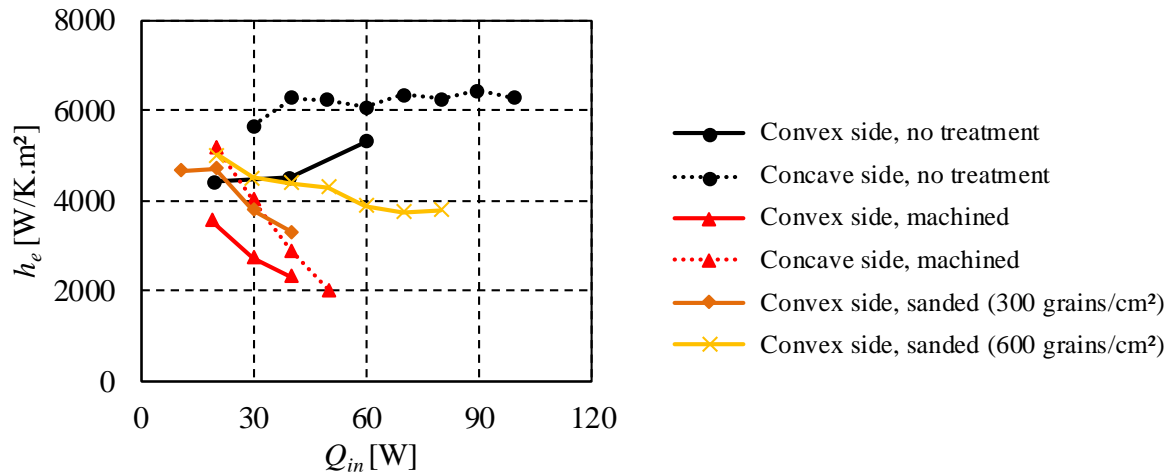


Figure 6: Influence of the surface quality on the heat transfer coefficient

Table 2: Characteristics and thermal performance of sample Cu-7-c after each surface treatment

Surface treatment	side	e_w [mm]	K [10^{-14} m^2]	$r_{p,eff}$ [μm]	Roughness [μm]	$Q_{opt,exp}$ [W]	$Q_{opt,th}$ [W]	$\Delta T_{sh,max,exp}$ [K]	$\Delta T_{sh,max,th}$ [K]	$h_{e,opt}$ [$\text{W}/(\text{m}^2 \cdot \text{K})$]
No	convex	6.0	16.9	11.5	5	60	102	9.0	9.8	5310
No	concave				5	100		12.6		6280
Machined	convex	5.5	19.5	11.5	40	40	128	12.6	9.8	2510
Machined	concave				40	50		20.2		2020
Sanded (300 g/cm ²)	convex	4.2	18	11.5	20	40	153	9.6	9.8	3320
Sanded (600 g/cm ²)	convex	4.0	26.8	11.5	15	80	229	16.7	9.8	3810
Polished with Lamplan	convex	3.9	0.43	7.1	5	50	-	16.8	-	2370

The three observed levels of thermal performance mentioned previously can be explained by the modification of the contact between the porous wick and the evaporator wall. If the sample is not flat, a gap is created between these two components. Figure 7 shows the three main configurations that can be encountered: a flat porous wick (a), a convex surface, creating a small gap (b), and a concave surface creating a large gap (c).

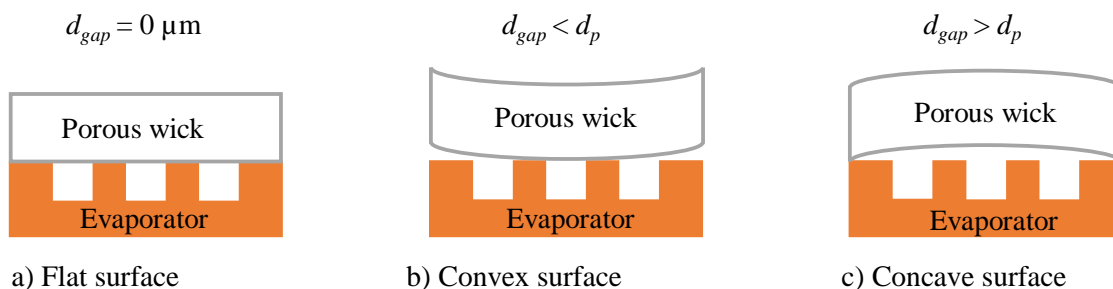


Figure 7: Schematic of the contact configurations between the wick and the evaporator wall

The gap size determine the boiling dynamics and the fluid flow between the porous wick and the evaporator wall. At low heat loads, a liquid phase may exist between the porous wick and the evaporator fin. Moreover, the meniscus may be located between the fin and the porous wick as shown in Figure 8 (a), as proposed by Demidov and Yatsenko [18]. When the heat load increases, a vapour bubble can be located between the fin and the porous wick (Figure 8b). If the pore diameter d_p is larger than the gap thickness d_{gap} , the vapour will be evacuated by the wick instead of the gap. Indeed, the meniscus remains at the location having the smallest pore diameter since the pressure difference is more difficult to overcome. This phenomenon leads to a partial dry out of the wick and to a large increase of the thermal resistance. Thus, $h_{e,opt}$ decreases, increasing the evaporator temperature, and if the heat load is increased, Q_{opt} is reached. This is even worse if the porous wick is flat and if there is no gap. At the contrary, if d_p is smaller than d_{gap} , the vapour is evacuated to the vapour grooves and the device operates correctly.

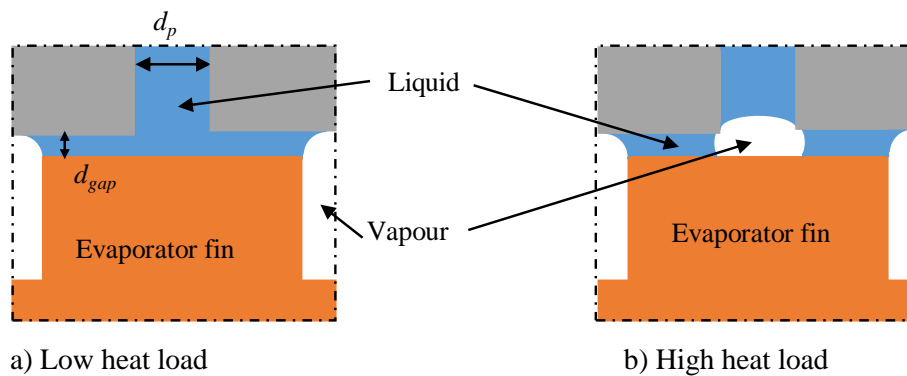


Figure 8: Schematic of the boiling dynamics at the vicinity of an evaporator fin

As a conclusion, the presence of a gap between the fins and the porous wick, when larger than the pore diameter, increases both the optimum heat flux and the heat transfer coefficient. That was also demonstrated by Platel *et al.* [11] about the start up, but it can be extended to moderate and high heat loads. The influence of the roughness of the surface seems deemed by the influence of the flatness and no conclusions can be drawn for this parameter.

3.1.4 Effect of the surface coating on the evaporator thermal behaviour

In order to study the effect of the wettability and hardness of the surface on heat transfer, the influence of a thin gold layer added by coating on the two zirconia porous samples performed. A thin layer of gold was deposited on the concave side of sample Zi-1 and on the convex side of sample Zi-2, in contact with the evaporator fins. The samples were tested before and after the coating with water as the working fluid.

Figure 9(a) shows the evolution of the heat transfer coefficient of the concave side of sample Zi-1 as a function of the heat load, before and after the coating. The difference between the two curves is not significant compared to the uncertainties. It means that the gold coating has no influence on the evaporator temperature. However, the optimum heat load reaches 130 W with the coating whereas it reaches only 80 W without it. Thus, the coating has a positive influence on Q_{opt} despite the poor contact between the concave wick surface and the wall, only at the edge of the copper block. This tendency is not fully understood at yet; it may be caused by several physical phenomena. First, due to the high thermal conductivity of gold (315 W/(m·K)) and to its low hardness, the layer of gold could act as an interstitial material, enabling to reduce the thermal contact resistance between the evaporator wall and the zirconia wick. For the same evaporator temperature, the temperature at the surface of the wick would be lower, and the occurrence of the nucleation would be delayed. Another possible explanation is linked to a wettability effect. If the contact angle gold/water would be smaller than the zirconia/water one, the onset of nucleate boiling would also be delayed due to the higher superheat required to activate the nucleation sites. These effects, or a combination of them, could explain why the gold coating provides a higher optimum heat load without increasing the heat transfer coefficient.

Figure 9(b) shows the thermal behaviour of the convex side of sample Zi-2 before and after the coating. The heat transfer coefficient is higher with coating as well as the optimum heat load (120 W compared to 110 W before coating). The maximum superheats are similar (68.9 K and 69.6 K after and before coating,

respectively). In this case, since a larger part of the wick surface is in contact with the evaporator, the significant decrease of the thermal contact resistance between the wall and the wick favourably affects the evaporator heat transfer coefficient, much more than the optimum heat flux value. It is interesting to observe that for a zirconia wick, the coating reduces the strong effect of the surface topography on the optimum heat flux value.

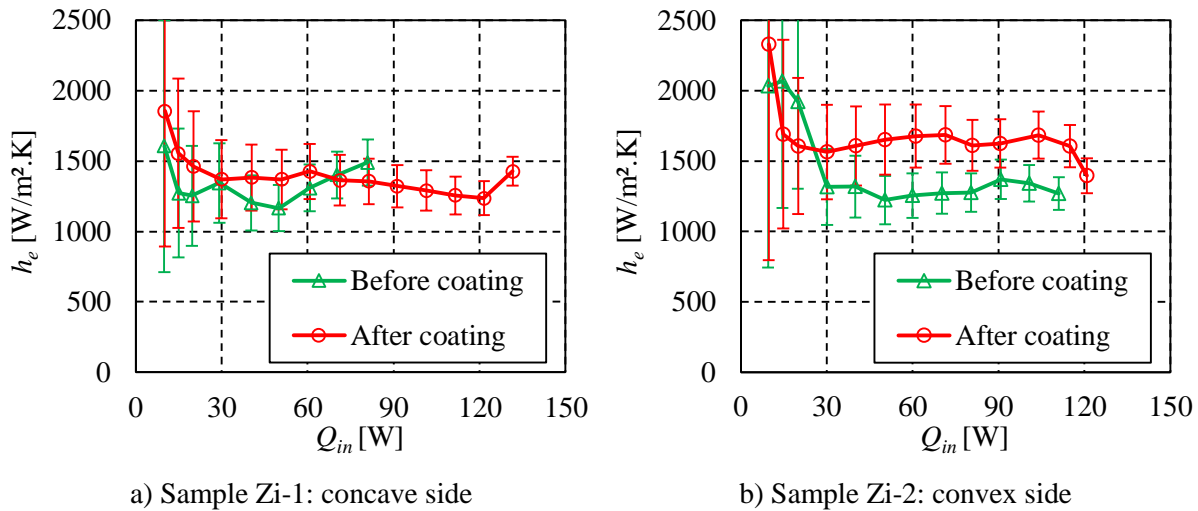


Figure 9: Comparison of the heat transfer coefficients before and after the coating

3.2 Datamining analysis with the complete database

The parametric study based on the comparison of samples having similar properties but with different surface properties shows that various phenomena can affect the heat transfer and that there is a strong coupling between them. In order to have a global comparison of the influence of the whole investigated parameters - surface topography, wettability, permeability, effective pore radius, thickness, and fluid properties - on the evaporator heat transfer coefficient at the optimum heat flux, a data mining method applied to the results obtained with the whole set of manufactured samples is proposed in the present section. The data used for the data mining are summarized in appendix. Since a great number of tests results are available, the statistical analysis may help to differentiate the influent parameters from the non-influent ones.

3.2.1 Description of the methodology

The selected method (called SPRINT) is a decision-tree-based classification. The classification starts by the building of a table containing several tests (lines) and for each test, several parameters (columns) as well as the test results. The test results are assigned to a given level (high, medium and low) depending on thresholds. The algorithm starts with the whole data set. The data set is partitioned according to a splitting criterion into subsets. The procedure is repeated recursively for each subset until each subset contains only members belonging to the same level or is sufficiently small. Shafer *et al.* [19] present in more details this scalable parallel classifier for data mining.

Fifty-three tests were performed with the porous samples, 29 and 24 with pentane and water, respectively, 39 and 14 on samples without and with surface treatment, respectively. The tests are classified depending on the optimum heat transfer coefficient $h_{e,opt}$, and on the chosen thresholds: 3000 W/(m²·K) and 5000 W/(m²·K). If $h_{e,opt}$ varies from 0 to 3000 W/(m²·K), the performance is considered as LOW, if it varies from 3000 to 5000 W/(m²·K), it is considered as MEDIUM and if it is higher than 5000 W/(m²·K), it is considered as HIGH. Then, the software is run. Firstly, it finds the most discriminating parameter and creates two branches in which the tests are classified according to the three levels. The branch which includes the tests leading to the major part of low heat transfer coefficients is not studied. The other branch, with the tests leading to the major part of high $h_{e,opt}$, is further investigated. The software finds another parameter that discriminates the remaining tests. Two more branches are built. At the end, the software is not able to find a discrimination of parameter anymore.

3.2.2 Results and analysis with the whole tests

The results of the data mining analysis with the whole test is presented on Figure 10. The first branch shows that the fluid is the most discriminating parameter. Indeed, all the tests leading to a high $h_{e,opt}$ value are obtained with pentane whereas twenty-three tests among the thirty-four leading to a low $h_{e,opt}$ are obtained with water. The second most discriminating parameter is the surface treatment: a surface treatment induces a low $h_{e,opt}$ in almost each case whereas it remains often at a high value without surface treatment. This result confirm the preponderant effect of the presence of a gap between the porous wick and the evaporator wall, which was suppressed with the applied surface polishing. Finally, the effective pore radius is the third discriminating parameter: an effective pore radius lower than around 15 μm leads to a higher heat transfer coefficient. The other parameters (porosity, permeability, thickness, but also roughness and level of flatness) are thus found to be less influent than the three other parameters, which is surprising as we could expect that there may exist an optimum in terms of flatness or roughness that leads to the highest heat transfer coefficient.

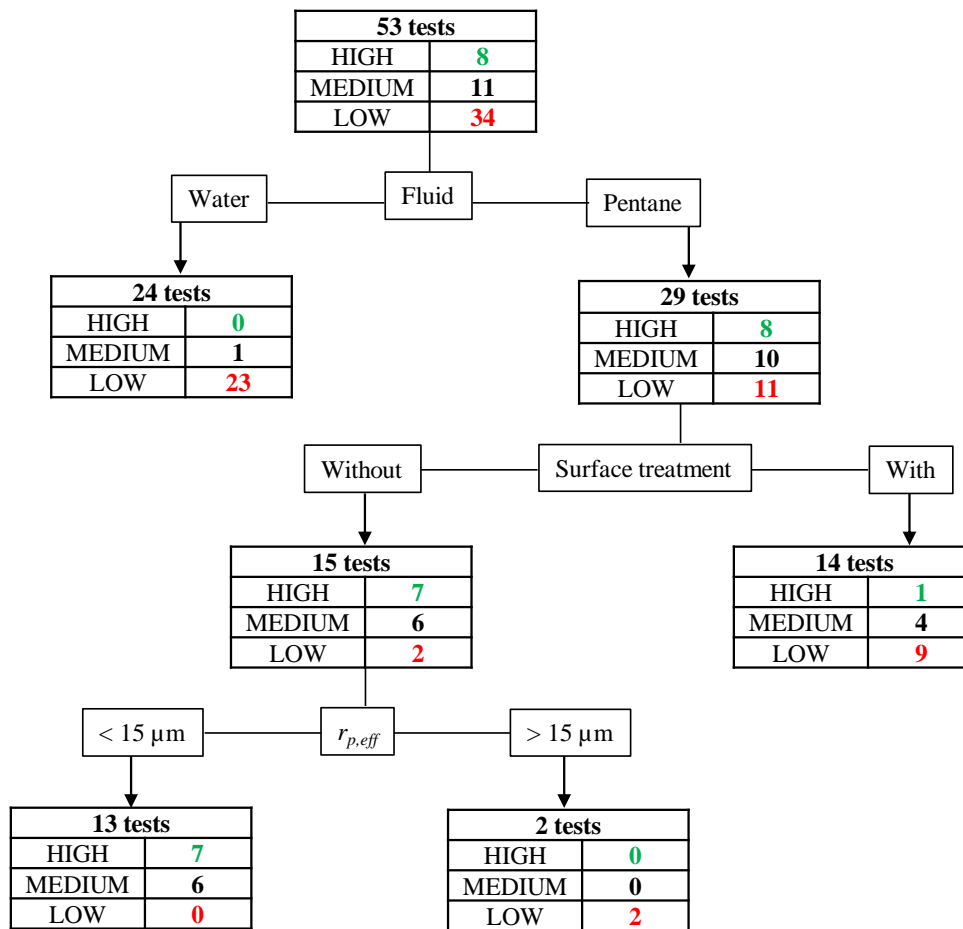


Figure 10: Decision tree for the heat transfer coefficient using the whole tests

3.2.3 Partial analysis of the tests conducted with water

The previous decision tree does not consider the tests obtained with water, since they were excluded at the first step. In order to also investigate these tests, the software is run without the tests obtained with pentane. Moreover, the thresholds are decreased from 3000 W/(m²·K) and 5000 W/(m²·K) to 1600 W/(m²·K) and 1800 W/(m²·K). The results obtained in these conditions are presented in Figure 11 and are surprisingly different than the results obtained with the pentane. A low permeability seems to induce a high $h_{e,opt}$. Indeed, a low permeability, hence a low porosity may increase the effective thermal conductivity of the porous medium. Then, the flatness of the samples is the most discriminating parameter. However, it is not easy to analyse because the major part of the tests leading to poor performance is obtained with the flat samples (5 tests among 8), but the major part of the tests leading to the best performance is also obtained with these samples (3 tests among 5). The same problem is observed with the thickness. This is the limit of this type of data analysis. Indeed, if no parameter is significantly discriminating, the results are not exploitable.

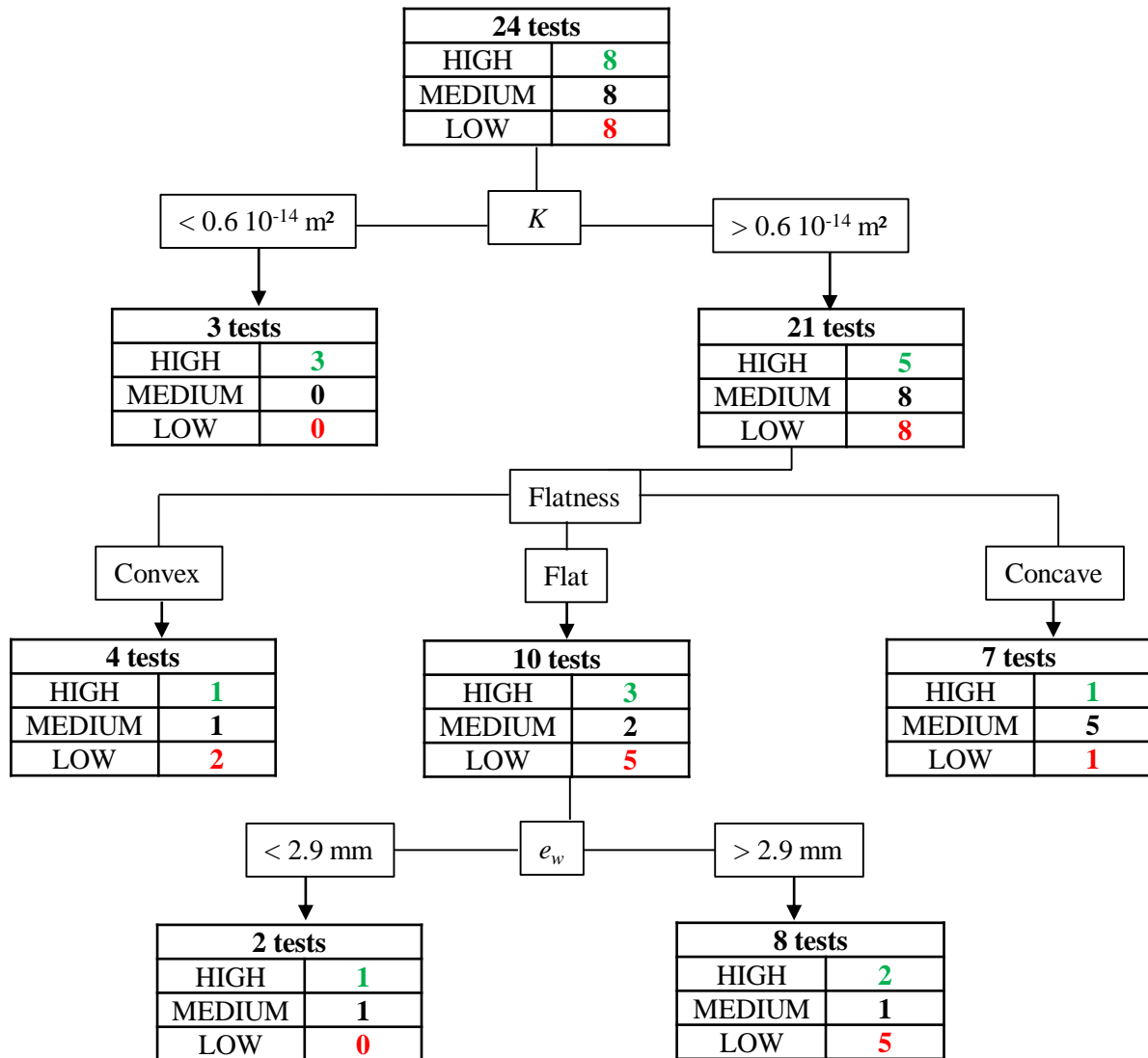


Figure 11: Decision tree for the heat transfer coefficient using the tests with water

As a conclusion, these decision trees must be seen as a tool enabling to hierarchize the importance of the various parameters affecting the heat transfer. Even if the limited number of test can affect the robustness of the method, it is interesting to note that the conclusions are drastically different between pentane and water. With the pentane, the heat transfer seems to be strongly affected by the surface treatment whereas with water, other phenomena, maybe linked to the hydrodynamic behaviour of the fluid, seems to have a stronger impact. This conclusion highlights the need to multiply the number of experimental study, with various fluids, various materials and various types and sizes of the fins in order to understand all the couplings between the different phenomena and to be able to develop predictive models of heat transfer at the surface of a porous medium in contact with an evaporator wall.

4 Conclusions

The present experimental study is intended to better understand the thermal behaviour of a capillary flat disk-shaped evaporator dedicated to a LHP. A test bench is designed in order to measure the evaporator heat transfer coefficient and maximum heat flux corresponding to the occurrence of an operating limit. The influence of the properties of the cylindrical wick surface in contact with the evaporator fins on the thermal behaviour was investigated by several mechanical surface treatments on a porous copper sample and by coating two porous zirconia samples with a 75 μm thick gold layer, without changing the surface topography.

The manufacturing process used in this work led to samples with a convex and a concave side. It was shown that the concave surface in contact with the evaporator wall, creating a gap larger than the pore diameter, enables the vapour to flow along the grooves instead of penetrating the wick. A surface treatment must be avoided: it seems to drastically decrease the heat transfer coefficient as well as the optimum heat flux because of the reduction of the gap size. The gold coating has a positive influence on the optimum heat load of a zirconia sample with a concave surface, enabling to decrease the thermal contact resistance between the evaporator wall and the wick since gold has a higher thermal conductivity than zirconia and a lower hardness. In addition, the gold coating could favourably modify the wettability of the wick, delaying the occurrence of boiling. This effect was much less pronounced with a convex surface, for which the decrease of the thermal contact resistance induces a significant enhancement of the evaporator heat transfer coefficient. Furthermore, for a zirconia wick, the coating reduces the strong effect of the surface topography on the optimum heat flux. A data mining analysis based on a decision tree, performed on fifty-three tests, confirmed the preponderant influence of the surface quality on the heat transfer coefficient.

However, if the importance of the flatness of the surface is highlighted by the present study, the diversity of the tested configurations also highlight the importance of the other parameters (roughness, effective pore radius, permeability, wettability, fluid properties, ...) on the influence of the flatness itself. Very different phenomena seems to control the heat transfer depending on the experimental conditions and no general conclusion can be drawn as long as all these phenomena are not properly identified and their effect quantified. More experimental studies are thus required in order to diversify the test conditions. The present study also highlights the importance of performing parametric studies by modifying only one parameter after each other and to perform a complete thermal and hydrodynamic characterisation for each samples. Because of the numerous parameters that can be involved when manufacturing or processing a porous wick, and the numerous parameters than can be chosen to integrate the wick in a real LHP, one can expect a long way before being able to develop a complete predictive tool enabling to determine the performance of a LHP evaporator directly from the manufacturing parameters of the porous wick.

Acknowledgments

The Carnot Institute Ingenierie@Lyon is gratefully acknowledged for its financial support and Vasile-Marian Scuturici (LIRIS) is gratefully thanked for its help on the Data Mining method.

References

- [1] J. Ku, 'Operating Characteristics of Loop Heat Pipes', in *29th International Conference on Environmental System*, 1999, vol. 1999-01–2007, pp. 503–519.
- [2] Y. F. Maydanik, 'Loop heat pipes', *Appl. Therm. Eng.*, vol. 25, pp. 635–657, 2005.
- [3] A. Faghri, *Heat pipe science and technology, Second Edition*. Global Digital Press, 2016.
- [4] C. C. Yeh, B. H. Liu, and Y. M. Chen, 'A study of loop heat pipe with biporous wicks', *Heat Mass Transf.*, vol. 44, no. 12, pp. 1537–1547, 2008.
- [5] R. Giraudon, S. Lips, D. Fabregue, L. Gremillard, E. Maire, and V. Sartre, 'Design and optimization of the sintering process of a bi-layer capillary structure for loop heat pipes', *Heat Pipe Sci. Technol. Int. J.*, vol. 8, no. 1, pp. 27–49, 2017.
- [6] R. Giraudon, S. Lips, D. Fabregue, L. Gremillard, E. Maire, and V. Sartre, 'Effect of the wick characteristics on the thermal behaviour of a LHP capillary evaporator', *Int. J. Therm. Sci.*, vol. 133, pp. 22–31, 2018.
- [7] Y. F. Maydanik, M. A. Chernysheva, and V. G. Pastukhov, 'Review: Loop heat pipes with flat evaporators', *Appl. Therm. Eng.*, vol. 67, no. 1–2, pp. 294–307, Jun. 2014.
- [8] J. Choi, B. Sung, C. Kim, and D.-A. Borca-Tasciuc, 'Interface engineering to enhance thermal contact conductance of evaporators in miniature loop heat pipe systems', *Appl. Therm. Eng.*, vol. 60, no. 1–2, pp. 371–378, 2013.
- [9] M. Khammar, D. Ewing, C. Y. Ching, and J. S. Chang, 'Heat transfer from a surface into a confined gap over a saturated porous plate', *Int. J. Heat Mass Transf.*, vol. 76, pp. 144–152, 2014.
- [10] M. J. Schertzer, D. Ewing, and C. Y. Ching, 'The effect of gap distance on the heat transfer between a heated finned surface and a saturated porous plate', *Int. J. Heat Mass Transf.*, vol. 49, no. 21–22, pp. 4200–4208, 2006.
- [11] V. Platel, O. Fudym, C. Butto, and P. Briend, 'Coefficient de transfert, à l'interface de vaporisation, d'une boucle fluide diphasique à pompage thermocapillaire', *Rev Gén Therm*, vol. 35, pp. 592–598, 1996.
- [12] C. Figus, Y. Le Bray, S. Bories, and M. Prat, 'Heat and mass transfer with phase change in a porous structure partially heated: continuum model and pore network simulations', *Int. J. Heat Mass Transf.*, vol. 42, pp. 1446–1458, 1999.
- [13] P. Kumar, B. Wangaskar, S. Khandekar, and K. Balani, 'Thermal-fluidic transport characteristics of bi-porous wicks for potential loop heat pipe systems', *Exp. Therm. Fluid Sci.*, vol. 94, pp. 355–367, 2018.
- [14] K. Odagiri, M. Nishikawara, and H. Nagano, 'Microscale infrared observation of liquid–vapor interface behavior on the surface of porous media for loop heat pipes', *Appl. Therm. Eng.*, vol. 126, pp. 1083–1090, Nov. 2017.
- [15] J. Choi, Y. Yuan, W. Sano, and D.-A. Borca-Tasciuc, 'Low temperature sintering of copper biporous wicks with improved maximum capillary pressure', *Mater. Lett.*, vol. 132, pp. 349–352, Oct. 2014.
- [16] S. W. Chi, *Heat pipe theory and practice: a sourcebook*. Washington DC: Hemisphere Pub. Corp., 1976.
- [17] P. Griffith and J. D. Wallis, 'The role of surface conditions in nucleate boiling', Cambridge Massachusetts Institute of Technology, Division of Industrial Cooperation, 1958.
- [18] A. S. Demidov and E. S. Yatsenko, 'Investigation of heat and mass transfer in the evaporation zone of a heat pipe operating by the inverted meniscus' principle', *Int. J. Heat Mass Transf.*, vol. 37, no. 14, pp. 2155–2163, 1994.
- [19] J. Shafer, R. Agrawal, and M. Mehta, 'SPRINT: A scalable parallel classifier for data mining', in *22th Int. Conf. Very Large Data Bases*, Bombay, India, 1996, pp. 544–555.

Appendix: Test parameters used for the data mining analysis

Sample	ε [%]	K [10^{-14} m ²]	$r_{p,eff}$ [μ m]	e_w [mm]	Surface treatment	Flatness type	Flatness [μ m]	Roughness [μ m]	Fluid	$h_{e,opt}$ [kW/(m ² K)]
Cu-1-b	39.3	11.6	11.3	3.2	WT	Convex	100	15	Water	1.17
Cu-2-b	26.7	2.57	23	2.95	WT	Convex	250	30	Water	1.30
Cu-2-c	27.1	1.37	11.5	2.8	WT	Convex	300	15	Water	1.83
Cu-2-c	27.1	1.37	11.5	2.8	WT	Convex	300	15	Water	1.68
Cu-2-c	27.1	1.37	11.5	2.8	WT	Convex	300	15	Pentane	3.20
Cu-2-c	27.1	1.37	11.5	2.8	WT	Concave	-200	15	Pentane	3.08
Cu-2-c	27.1	1.37	11.5	2.8	WT	Concave	-200	15	Pentane	3.75
Cu-2-c	27.1	1.82	18.5	2.7	S300	Concave	-50	5	Pentane	3.45
Cu-2-c	27.1	1.82	18.5	2.7	S300	Concave	-50	5	Pentane	2.42
Cu-3-a	40.6	10.1	18.2	5.2	WT	-	-	10	Water	1.85
Cu-3-a	40.6	10.1	18.2	5.2	WT	-	-	10	Water	1.70
Cu-3-a	40.6	10.1	18.2	5.2	WT	-	-	10	Water	1.70
Cu-3-a	40.6	10.1	18.2	5.2	WT	-	-	10	Water	1.62
Cu-3-a	40.6	10.1	18.2	5.2	WT	-	-	10	Water	1.85
Cu-3-a	40.6	10.1	18.2	5.2	WT	-	-	10	Water	2.28
Cu-3-a	40.6	10.1	18.2	5.2	WT	-	-	10	Water	1.26
Cu-3-a	40.6	10.1	18.2	5.2	WT	Concave	-200	10	Pentane	1.92
Cu-3-a	40.6	10.1	18.2	5.2	WT	Convex	300	10	Pentane	2.06
Cu-4-a	22.6	0.6	5	4.7	WT	Convex	160	10	Water	1.06
Cu-4-a	22.6	0.6	5	4.7	WT	Convex	160	10	Water	2.40
Cu-4-a	22.6	0.6	5	4.7	WT	Convex	160	10	Water	1.52
Cu-4-a	22.6	0.6	5	4.7	WT	Convex	160	10	Pentane	5.40
Cu-4-a	22.6	0.6	5	4.7	WT	Convex	160	10	Pentane	5.20
Cu-4-a	22.6	0.12	5	4.45	P	Flat	50	5	Pentane	1.42
Cu-4-a	22.6	0.12	5	4.45	P	Flat	50	5	Pentane	3.01
Cu-5-a	37	10.5	10.2	2	WT	Concave	-60	5	Water	1.58
Cu-5-a	37	10.5	10.2	2	WT	Concave	-60	5	Water	1.61
Cu-5-a	37	10.5	10.2	2	WT	Concave	-60	5	Water	1.70
Cu-5-a	37	10.5	10.2	2	WT	Concave	-60	5	Pentane	5.25
Cu-5-a	37	10.5	10.2	2	WT	Convex	270	5	Pentane	5.03
Cu-5-a	37	10.5	10.2	2	WT	Convex	270	5	Pentane	5.03
Cu-5-a	37	10.5	10.2	2	WT	Convex	270	5	Pentane	4.77
Cu-5-a	37	0.26	5	1.9	S300	Flat	0	10	Pentane	2.57
Cu-5-a	37	0.26	5	1.9	S300	Flat	0	10	Pentane	2.59
Cu-5-a	37	3.25	30.7	1.9	A	Flat	0	10	Pentane	5.84
Cu-5-a	37	3.25	30.7	1.9	A	Flat	0	10	Pentane	2.30
Cu-6-c	28.6	0.52	9.2	2.1	WT		-	10	Water	1.95
Cu-7-b	37	18.8	52.1	5.6	WT		-	-	Water	0.84
Cu-7-c	41.8	16.9	11.5	6	WT	Convex	350	5	Water	1.26
Cu-7-c	41.8	16.9	11.5	6	WT	Concave	-150	5	Water	1.66
Cu-7-c	41.8	16.9	11.5	6	WT	Concave	-150	5	Water	1.77
Cu-7-c	41.8	16.9	11.5	6	WT	Convex	350	5	Pentane	7.05
Cu-7-c	41.8	16.9	11.5	6	WT	Concave	-150	5	Pentane	6.28
Cu-7-c	41.8	19.5	11.5	5.8	M	Flat	0	40	Pentane	2.51
Cu-7-c	41.8	19.5	11.5	5.8	M	Flat	0	30	Pentane	2.02
Cu-7-c	41.8	18	11.5	4.45	M	Convex	60	20	Pentane	3.32
Cu-7-c	41.8	26.8	11.5	4.2	S600	Convex	320	15	Pentane	3.81
Cu-7-c	41.8	0.43	7.1	4	P	Flat	0	5	Pentane	2.37
Cu-7-c	41.8	0.43	7.1	4	P	Flat	0	5	Pentane	1.86
Cu-8-a	22.4	0.56	11.3	5.45	WT	Convex	200	5	Pentane	4.38
Cu-8-a	22.4	0.56	11.3	5.45	WT	Concave	-80	5	Pentane	3.75
Cu-8-a	22.4	0.56	11.3	5.45	WT	Concave	-80	5	Water	2.00
Cu-8-a	22.4	0.56	11.3	5.45	WT	Convex	200	5	Water	3.00

WT: Without surface treatment; S300/S600: Sanded with a grain density of 300/600 gr/cm²

P: Polished with the Lamplan polisher; M: Machined with the turning machine; A: Immersed in an acidic solution

Nomenclature

h	heat transfer coefficient	$\text{W.m}^{-2}.\text{K}^{-1}$
H	Height	m
I	electrical current	A
K	permeability	m^2
P	pressure	Pa
Q	heat flux	W
r	radius	m
S	cross-sectional area, or surface	m^2
T	temperature	K
U	voltage	V

Greek Symbols

Δ	difference	-
ρ	density	kg.m^{-3}

Subscripts

e	evaporator
eff	effective
elec	electrical
exp	experimental
gap	gap
hs	hydrostatic
in	input
l	liquid
loss	heat losses by the back face of the evaporator
max	maximum
NCG	non-condensable gases
opt	optimum
p	pore
sat	saturation
sh	superheat
th	theoretical
v	vapour
vt	vapour tube
w	wick